ORIGINAL PAPER

Post-polymerization reactivity of free radicals trapped in resin-based dental restorative materials by ESR spectroscopy

Bruna Cristina Amorim[1] · Bruno Luiz Santana Vicentin[1] · Eduardo Di Mauro[1]

Abstract

The propagating and allylic free radicals generated when polymerizing dimethacrylate resin-based materials used in dentistry are detected by electron spin resonance (ESR) spectroscopy as a nine-line spectrum. This study aimed to probe their post-polymerization reactivity with a novel methodology to quantify these radicals separately. X-band ESR spectra were recorded from a photo-cure dental resin composite (~ 20 days) and a dual-cure resin cement (~ 15 days). Spectra simulations were applied to separate and determinate the contribution from each radical to the ESR signal according to the method presented. The decay curves of the free radicals were then obtained to probe their post-polymerization reactivity as function of composition and initiation mode (photo-cure and self-cure). The allylic radical's post-polymerization half-life time was approximately twice than that of the propagating radical, independently the composition and the activation mode, indicating that their relative reactivity does not depend of these parameters. The methodology presented for individual quantification of free radicals showed to be adequate to probe the kinetics of the free radicals generated and trapped in resin-based dental.

Introduction

Resin composites and resin cements based on bifunctional dimethacrylates monomers are widely used in dentistry. For example, dental resin composites (DRCs) are used in direct restoration of the lost part of the tooth, recovering its function and aesthetics, while resin cements (RCem) are indicated for indirect restorations

✉ Bruno Luiz Santana Vicentin
bruno.vicentin@uel.br

1 Laboratory of Electron Paramagnetic Resonance, Department of Physics, State University of Londrina, C. P. 6014, Londrina, PR 86051-990, Brazil

and cementation of an intraradicular post, which will assist the retention of the external restoration [1–5].

The polymerization reaction of dental restorative materials may occur at oral temperature and is usually initiated by physical activation (photo-cure) or chemical activation (self-cure). The DRC's mass is exposed inside the oral cavity; thus, the majority of the DRCs are photo-cured. These materials contain the initiator camphorquinone (absorption peak at approximately 470 nm) and tertiary amines (co-initiators) [6–10], which interacts with the excited camphorquinone to form the free radicals that will initiate the chain reaction of polymerization [11]. On the other hand, the RCem's mass is, in some cases, totally inserted inside the root canal; thus, self-cure is chosen for these materials. The self-cure occurs by oxidation reaction of an organic peroxide (like benzoyl peroxide) and a tertiary amine when the base paste and catalyst are mixed [10]. In addition, some dental materials mix photo-cure to self-cure in order to obtain greater degree of conversion at deepest points of a restoration, such as dual-cure resin cements, used for cementing translucent fiberglass posts inside the root canal [5, 12].

After polymerization, unreacted free radicals are trapped in the polymer matrix due to vitrification [11, 13–16]. Truffier-Boutry et al. [11] proposed that the free radicals generated and trapped in the network during photo-cure of DRCs are the propagating (RI), the methacrylate (RII) and the allylic (RIII) radicals. Furthermore, they proposed that only RI and RIII are responsible for the formation of the nine-line electron spin resonance (ESR) spectrum of the DRCs, because RII reacts rapidly or the quantity generated is too small to be detected [11].

The results obtained by Truffier-Boutry et al. [11] have been confirmed by multifrequency (X-, Q- and W-bands) ESR experiments and spectra simulations [14]. In addition, Vicentin et al. [12] showed that for both DRC and RCem, the radical species generated and trapped are the same, and that the nine-line ESR signal of the free radicals detected is independent on the initiation mode [15].

All these researches are based on ESR spectroscopy, which is a nondestructive technique that allows identification of paramagnetic species, such as free radicals [17, 18]. In addition, ESR spectroscopy allows to observe the signal of the free radicals trapped in the matrix after polymerization because the free radical signal persists even long time after initiation [16, 19–24]. The ESR signal is very intense in the first minutes after initiation, and although it decreases when the polymerization reaction stops, it is still detected 70 days after initiation [20, 21]. Truffier-Boutry et al. [25] assigned this decrease in the ESR signal after polymerization of the shrinkage phenomenon linked to the free volume relaxation in the organic matrix, resulting in increased proximity and mobility of the radical species [25].

The macroradicals entrapped in the vitrified matrix of dental resinous materials have been widely studied, and their structure is already determined as mentioned, but their reactivity and half-life time are not completely described and understood. Leprince et al. [16, 24] studied the kinetic of RI and RIII free radicals trapped in DRCs stored in different environments and under different irradiation modes, but using a methodology that does not allow complete separation of the free radicals for further analysis.

The understanding of the post-polymerization phenomena yields formulation of more efficient materials, especially for the dental materials area, where the aesthetic, quality and longevity of the restoration are required. Therefore, this research aimed to propose a novel methodology to construct the decay curve of the propagating and allylic radicals separately and probe their post-polymerization reactivity in the vitrified matrix. The null hypotheses of this study were: The reactivity of the free radicals is not different; the kinetics is not dependent on the composition and initiation mode.

Materials and methods

Resin and cement utilized and experimental methodology

The Filtek™ Z350 XT photopolymerizable resin composite from 3M ESPE and the dual-cure resin cement Allcem from FGM were used. The monomers and inorganic fillers contained in these materials are shown in Table 1. These materials were chosen because they allow analysis of the influence of the composition and the initiation mode on the concentration of free radicals with time. Thus, ESR experiments were separated in three groups: photo-cured DRC, photo-cured RCem and self-cured RCem.

The X-band ESR experiments were performed using a JEOL (JES-PE-3X) spectrometer at room temperature, 0.32 mT modulation amplitude and 100 kHz modulation frequency. An internal standard of MgO:Mn^{2+} was used as the magnetic field marker and intensity standard. DRC and RCem samples were inserted in a Teflon matrix (6 mm height and 4 mm in inner diameter). The photo-cured samples were irradiated for 40 s (492 mW/cm^2 power) with a LED device Emitter A (Schuster, Santa Maria, RS, Brazil). After the irradiation, the photo-cured DRC and RCem samples were inserted into the spectrometer cavity for immediate analysis. For the self-cured RCem specimen, the experiment started 7 min after mixing the two pastes into the Teflon matrix (curing time of the material when using self-cure only, according to manufacturer).

After the cure of the composites, ESR spectra were recorded for ~500 h from DRC (~20 days) and ~350 h from RCem (~15 days) samples. For all groups,

Table 1 Information about the composition of the restorative materials according to the manufacturer

	Monomers	Inorganic fill	Filler content (wt%)	Shade
Filtek™ Z350 XT	Bis-GMA, UDMA, TEGDMA and bis-EMA	Silica and zirconia nanoparticles; aggregated zirconia/silica nanoparticles microclusters	78.5	A2B
Cement Allcem	Bis-GMA, bis-EMA, TEGDMA	Barium–aluminosilicate glass microparticles and silicon dioxide nanoparticles	68	A2

spectra were acquired every 5 min in the first 24 h and every 10 min in the next 24 h. From the third day onwards, on average 12 spectra per day were recorded. The spectra with poor signal-to-noise ratio leading to peak measurement with low accuracy were disregarded.

One spectrum a day per group was chosen as reference for simulation with the WinEPR (Bruker) software. All spectra were analyzed, and the curves of relative concentration of RI and RIII were constructed with the Origin Pro 8 software following the methodology described in the next section.

Methodology to investigate the relative concentration of propagating and allylic radicals

The structure of the free radicals RI and RIII detected by ESR spectroscopy in photo-cured and self-cured bifunctional dimethacrylate resin-based composites is shown in Fig. 1. R denotes the differential part of the monomer, and A denotes the differential part of the amine.

The spectra simulations were made by overlapping simulations from RI and RIII radicals. For RI radical, the first neighbors of the unpaired electron are $CH_3 - C^{.} - CH_2$, so the simulations were performed considering the hyperfine interactions between unpaired electron and three equivalent protons from the hydrogen atoms from the CH_3 group and two non-equivalent protons from the hydrogen atoms from the CH_2 group. For RIII radical, the unpaired electron interacts with $CH_2 - C^{.} - CH_2$; thus, the simulations were obtained considering the hyperfine interactions of the unpaired electron with four equivalent protons from the hydrogen atoms of two CH_2 groups [11, 14, 15].

The spin Hamiltonian for RI and RIII is $H(RI) = g\beta HS + [AIS + BIS + CIS]$ and $H(RIII) = g\beta HS + [AIS + BIS]$, respectively, with $g\beta HS$ the Zeeman effect term and AIS, BIS and CIS the terms referring to hyperfine interactions of first and second order [11, 14, 15]. As the third and fourth lines of the field marker overlaps with the DRC and RCem spectra, the marker was also simulated.

Figure 2 shows the results of simulation of the field marker, RI radical, RIII radical and the overlap of the simulated "RI + RIII + field marker" spectra with the characteristic nine-line ESR signal obtained from photo-cured DRC. Figure 2 indicates the fourth line as L_4 and center line as LC(exp) in the experiment signal. It is

Fig. 1 Propagating (RI) and allylic radicals (RIII) generated during polymerization of photo-cure or self-cure dimethacrylate resin-based composites
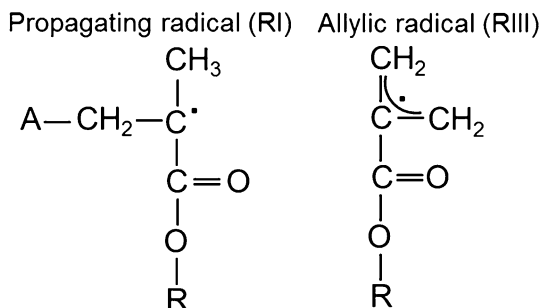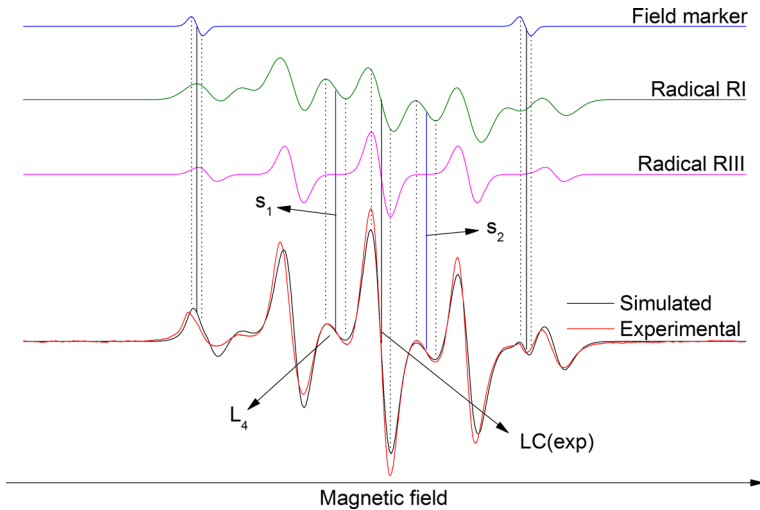
Fig. 2 Simulation of the field marker spectra MgO/Mn^{2+}, radical RI, radical RIII and the sum of the simulations providing a typical ESR spectrum obtained through the experiment

possible to see that the center line in the experiment signal is a superposition of the center lines from RI and RIII free radicals, obtained by simulation (vertical center line) [11, 14, 15]. In addition, it is concluded that the fourth and sixth lines from experiment signal are originated from RI free radical only (s_1 and s_2 vertical lines). In this way, we can say that the fourth and sixth lines are "single lines" arising only from RI, and the fifth line is a "mixed line," generated by superposition of RI and RIII. These characteristics were observed in all simulations for the three groups studied and are in accordance with Truffier-Boutry et al. [11], Fontes et al. [14] and Vicentin et al. [15].

Since L_4 from experiment signal is nothing more than the fourth line from RI radical, the peak-to-peak intensity of L_4 in all the experiment signals was used to estimate the relative concentration of RI. We may now find a way to estimate the relative concentration of RIII in the composite separately. The methodology proposed is as fallows.

From Fig. 2, we can observe that

$$LC(exp) = LC(RI) + LC(RIII), \tag{1}$$

where LC(exp) is the peak-to-peak intensity of center line from the experiment signal, LC(RI) the peak-to-peak intensity of center line from simulated RI, and LC(RIII) the peak-to-peak intensity of center line from simulated RIII. Assuming that the center line from simulated RI is α times more intense than its fourth line:

$$LC(RI) = \alpha L_4. \tag{2}$$

Substituting Eq. (2) into Eq. (1),

$$LC(RIII) = LC(exp) - \alpha L_4. \tag{3}$$

The LC(exp) and L_4 intensities are determined from experiment, while the α value is obtained from the simulations of RI by measuring the ratio LC(RI)/L_4 of the peak-to-peak intensities. Thus, Eq. (3) gives the peak-to-peak intensity of the center line from RIII, which can be used to estimate the relative concentration of RIII free radicals in the sample. This methodology allows quantification of RI and RIII in the composite analyzed separately, since α is known.

Results

Figures 3, 4 and 5 show the simulated spectra from RI and RIII and the overlapping of these simulations with the field marker and the experiment obtained spectra for the photo-cured DRC, photo-cured RCem and self-cured RCem.
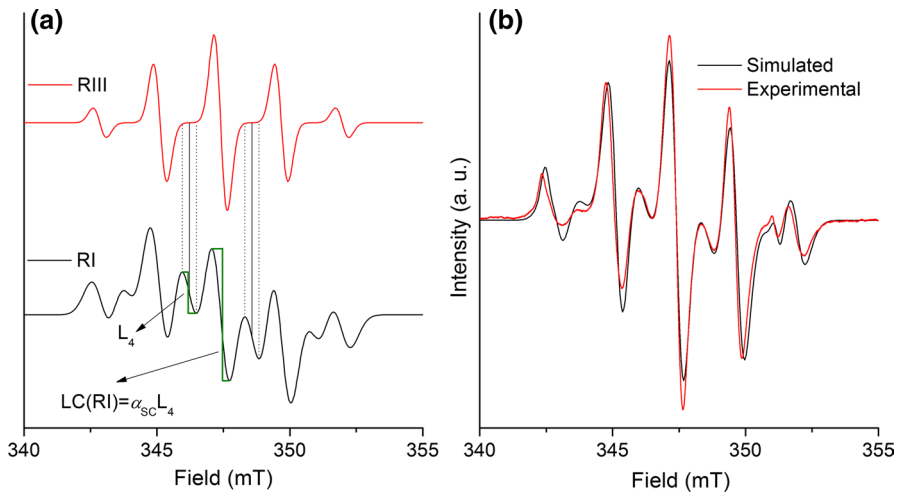
Table 2 provides the spectroscopic parameters used for simulations of the RI and RIII radicals for the photo-cured DRC, photo-cured RCem and self-cured RCem. The proportionality constant α obtained from simulations of RI (indicated in Figs. 3, 4, 5) and the hyperfine coupling constants (hfcc) used for the simulations of RI are given in Table 3. In Table 3, A is the hfcc for the three equivalent protons from the CH_3 group, B is the hfcc for one proton from CH_2, and C is the hfcc for the second proton from the same CH_2 group. In the end of Table 3 are shown the values of the peak-to-peak intensity of the lines LC and L_4 obtained from the simulations of the RI on different days. Table 4 gives the hfcc for the simulation from RIII, where A is the hfcc for the two equivalent protons from the first CH_2 group and B the hfcc for two equivalent protons from the second CH_2 group. As the protons from the hydrogen atoms near the unpaired electron in the RIII radical were considered as equivalent, the constants A and B were set equal.
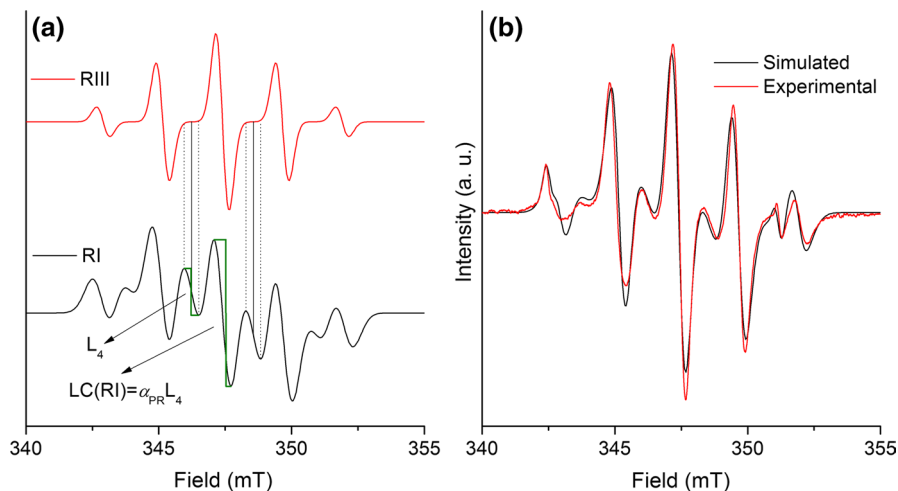
Fig. 3 Simulated spectra of RI and RIII (**a**) and overlapping of the RI, RIII and field marker simulations with the experimentally obtained spectrum using the photo-cured dental resin composite sample (**b**)
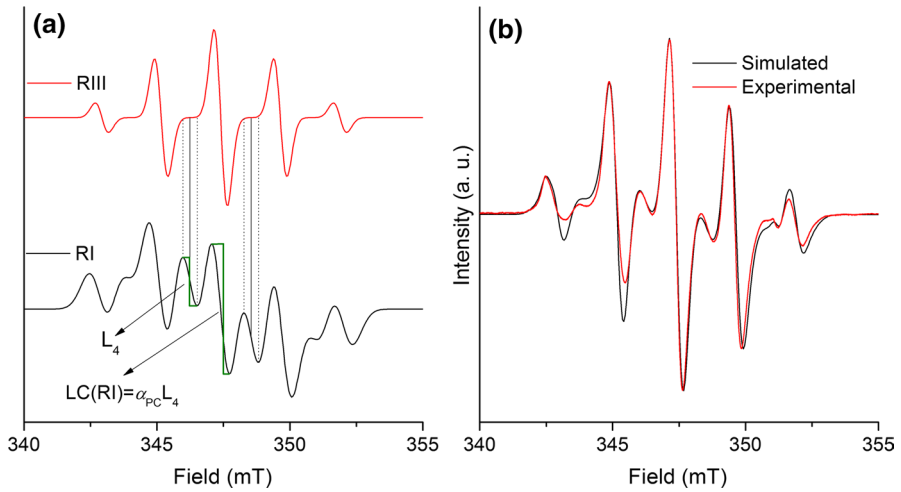
Fig. 4 Simulated spectra of RI and RIII (**a**) and overlapping of the RI, RIII and field marker simulations with the experimentally obtained spectrum using the photo-cured resin cement sample (**b**)

Fig. 5 Simulated spectra of RI and RIII (**a**) and overlapping of the RI, RIII and field marker simulations with the experimentally obtained spectrum using the self-cured resin cement sample (**b**)

Table 2 Spectroscopic parameters used for the simulations of RI and RIII radicals in the photo-cured dental resin composite, photo-cured resin cement and self-cured resin cement samples

	Spectroscopic factor	Line shape	Line width (mT)	θ	φ
RI	$g = 2.0051$	$L/G = 1$	$l_x = l_y = l_z = 0.8$	10	50
RIII	$g = 2.0051$	$L/G = 1$	$l_x = l_y = l_z = 0.5$	10	50

Table 3 Hyperfine coupling constants used for the simulations of the RI radical, values of the proportionality constants α and peak-to-peak intensity of the lines LC and L_4 obtained from the simulations
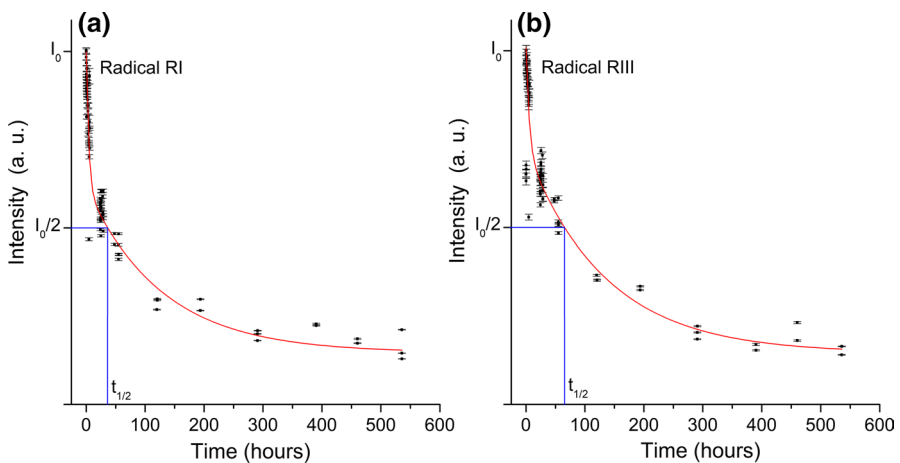
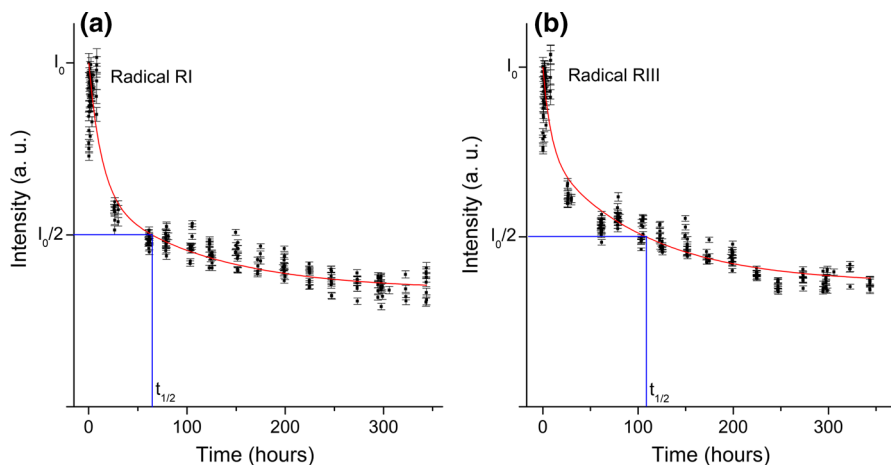| Component	Photo-cured dental resin composite			Photo-cured resin cement			Self-cured resin cement		
	$A/g\beta$ (mT)	$B/g\beta$ (mT)	$C/g\beta$ (mT)	$A/g\beta$ (mT)	$B/g\beta$ (mT)	$C/g\beta$ (mT)	$A/g\beta$ (mT)	$B/g\beta$ (mT)	$C/g\beta$ (mT)
(x, x)	2.20	1.40	1.00	2.20	1.20	1.00	2.30	1.30	1.00
(x, y)	0	0	0	0	0	0	0	0	0
(x, z)	0	0	0	0	0	0	0	0	0
(y, y)	2.20	1.40	0.90	2.20	1.20	0.95	2.10	1.40	0.90
(y, z)	0	0	0	0	0	0	0	0	0
(z, z)	2.20	1.70	0.90	2.20	2.15	0.95	2.10	1.80	0.90
Proportionality constant	α_{PR} = 3.1			α_{PC} = 2.7			α_{SC} = 3.2		
Peak-to-peak intensity of ESR lines	LC (a.u.)		L_4 (a.u.)	LC (a.u.)		L_4 (a.u.)	LC (a.u.)		L_4 (a.u.)
Day 1	369.0		118.3	528.5		197.5	540.0		169.0
Day 2	222.8		71.4	348.0		130.0	353.2		110.5
Day 3	158.2		50.7	313.1		117.0	212.0		66.3
Day 6	83.2		26.7	314.7		117.6	227.1		71.0
Day 9	59.3		19.0	290.2		108.5	216.9		67.8

Table 4 Hyperfine coupling constants used for the simulation of the RIII radical

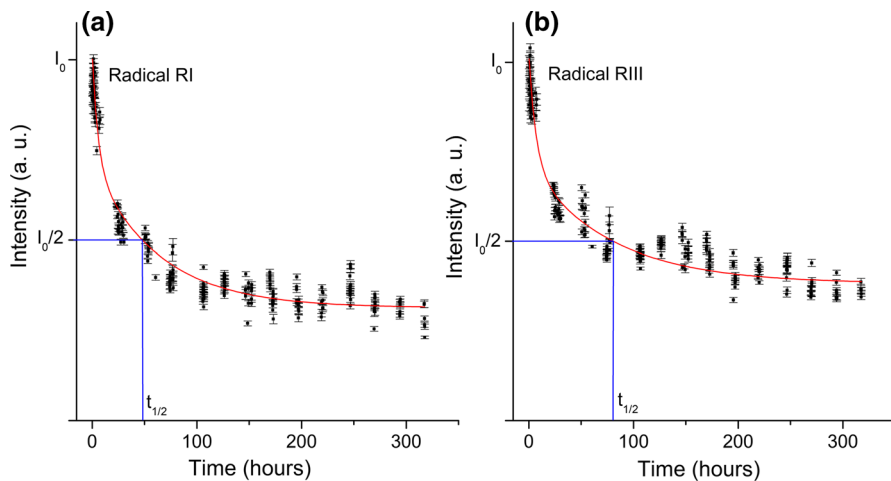| Component	Photo-cured dental resin composite		Photo-cured resin cement		Self-cured resin cement	
	$A/g\beta$ (mT)	$B/g\beta$ (mT)	$A/g\beta$ (mT)	$B/g\beta$ (mT)	$A/g\beta$ (mT)	$B/g\beta$ (mT)
(x, x)	2.25	2.25	2.24	2.24	2.28	2.28
(x, y)	0	0	0	0	0	0
(x, z)	0	0	0	0	0	0
(y, y)	2.25	2.25	2.24	2.24	2.28	2.28
(y, z)	0	0	0	0	0	0
(z, z)	2.25	2.25	2.24	2.24	2.28	2.28

The relative concentration of RI and RIII, obtained for the three groups analyzed using the methodology presented in this study, is shown in Figs. 6, 7 and 8. The half-life times from each radical were determined from the curve fitting (indicated in the graphs), and their values are shown in Table 5. The errors were estimated by the agreement between curve fitting and experimental points. RCem presented intense signal of radical, while DRC presented weak sign. Consequently, the number of spectra that offered a peak measurement with good accuracy was much higher from RCem. For this reason, there are more points in the RCem graphs.

Fig. 6 Decay in the concentration of RI (propagating) and RIII (allylic) on the photo-cured dental resin composite sample

Fig. 7 Decay in the concentration of RI (propagating) and RIII (allylic) on the photo-cured resin cement sample

Fig. 8 Decay in the concentration of RI (propagating) and RIII (allylic) on the self-cured resin cement sample

Table 5 RI and RIII radicals' half-life times

	$t_{1/2}$(RI) (h)	$t_{1/2}$(RIII) (h)	$t_{1/2}$(RIII)$/t_{1/2}$(RI)
Photo-cured dental resin composite	36.0 ± 1.8	65.5 ± 3.3	1.8 ± 0.2
Photo-cured resin cement	64.5 ± 3.9	108.7 ± 8.7	1.7 ± 0.2
Self-cured resin cement	47.8 ± 1.9	80.9 ± 8.1	1.7 ± 0.2

Discussion

The macroradicals RI and RIII generated during irradiation and/or entrapped in the vitrified matrix of dental resinous materials have been widely studied. Fontes et al. [14] reported quantification of the free radicals RI and RIII on a dental resin composite (Z100, 3 M ESPE) during irradiation 200 s irradiation by ESR spectroscopy. They found that the relative concentration of RIII grows rapidly during irradiation, reaching stabilization after 200 s with maximum intensity ~ 2400 (arbitrary units). On the other hand, the relative concentration of the RI radical grows very slowly, going from 0 to ~ 200 (arbitrary units) in the same time interval [14]. Leprince et al. [24] studied the kinetic of RI and RIII free radicals trapped in DRCs stored under different conditions (in air at 25 and 37 °C; in argon, oxygen and water at 25 °C). By quantifying the relative concentration of allylic radical (RIII), they found that the storage condition had no influence on the kinetics in the first day (0–24 h), but from 1 day to 1 month, the rate of decay depended on the storage environment. Leprince et al. [16] studied the irradiation mode's impact on radical entrapment by measuring the concentration of RI and RIII in photo-active resins. They reported that RI concentrations decrease at higher rates than RIII during the first 4 h [16].

All these studies concerning the quantification of propagating and allylic radicals used the central line of the characteristic nine-line ESR signal arising from methacrylate resin-based materials to probe the concentration of the allylic radical (RIII). However, the simulations in this research make it clear that the center line is actually the sum of the central lines from RI and RIII, which is in accordance with Vicentin et al. [15], Fontes et al. [14] and Truffier-Boutry et al. [11]. Therefore, the quantification of the RIII radical by measuring the peak-to-peak intensity of the central line in the ESR signal carries a contribution from the other radical present in the sample, which is not negligible. This research presented a methodology to remove this contribution. In addition, the quantification of the RI and RIII radicals in different materials under different initiation modes is presented in Figs. 6, 7 and 8. The decay curve obtained from each free radical allowed probing their post-polymerization reactivity and half-life time, as shown in Table 5.

Intense decay of the concentration of free radicals in the first 24 h for all groups analyzed (independent of the irradiation mode and/or composition) was observed. During approximately the first 24 h after light cure, volumetric shrinkage (which is linked to the free volume relaxation in the organic matrix) occurs, resulting in increased proximity and mobility of the radical species. Thus, the free radical trapped moves closer to each other, and the probability of termination increases due to shrinkage [25]. After that, although the termination becomes more restricted, the concentration of free radicals continues to decrease.

Table 5 shows the post-polymerization half-life time calculated from the decay curves to estimate their reactivity in the vitrified matrix. It is possible to see that the half-life time of RIII is always higher than that verified for RI. This is because the allylic radicals are unable to react with species other than free radicals

because of higher stability due to a resonance phenomenon. In contrast, the propagating radicals (RI) exhibit sufficient reactivity to interact also with remaining double bonds. In this way, additional propagation reactions can repeat locally, leading to some bimolecular radical termination through a reaction–diffusion-controlled termination mechanism [13, 25].

Table 5 shows that the absolute half-life time depends on the irradiation mode and composition of the material. This difference can be associated with intrinsic factors, such as the initiator system, fillers, viscosity and extrinsic conditions to the polymerization, as the amount of the sample to be polymerized, the ambient temperature at the time of polymerization and angle of incidence of the radiating source on the sample. This is in accordance with Leprince et al. [24], who attested that the fillers influenced on the radicals' kinetics [24]. Thus, comparing the photo-cured samples, the absolute half-life time obtained from RCem is approximately twice the verified for DRC, because the DRC has higher concentration of inorganic fillers. Comparing the self-cured RCem to photo-cured RCem, the absolute half-life time was greater for the photo-cured sample. It may be associated with the faster vitrification and higher number of free radicals resultant from the photo-cure reaction [22]. The self-cure reaction is much slower than photo-cure reaction [22], and the final polymer presents lower hardness [26, 27] and lower polymerization shrinkage [28]. These factors may have influenced on the post-polymerization reactivity of the trapped radicals, because the polymeric network in self-cured sample allowed fluidity and diffusion of the radical species, resulting in a higher rate of combination of paramagnetic species after polymerization.

We also studied the relative reactivity between the two free radicals to probe changes in the kinetics of the free radicals during time evolution. Table 5 shows that absolute reactivity of the free radicals is different (first and second columns), resulting in different kinetics and decay curves; however, we verified that the radicals continue to combine in the same proportion as the post-polymerization reaction occurs (3rd column). In addition, we found that the relative reactivity between free radicals was not influenced by the composition or by the activation mode because the $t_{1/2}(\text{RIII})/t_{1/2}(\text{RI})$ ratio was constant. This means that the environment did not influence the proportional "consumption" of free radicals.

Studying the concentration of free radicals in a long-time interval is limited by the high number of spectrum to be recorded and analyzed and the high number of simulations to be performed as well, which restricts the number of specimens to be evaluated. However, the methodology presented in this research simplifies this task and showed to be adequate to estimate the concentration of the allylic radical. This study is important because it assists future researches in the dental materials area to apply the ESR spectroscopy technique in their studies. In conclusion, the null hypotheses of this research must be rejected, because the post-polymerization half-lime time of the allylic radical was approximately twice the value verified for the propagating radical, and their kinetics was dependent on the composition and the initiation mode. However, their relative reactivity was constant.

Conclusion

Considering the limitations of this study, the methodology presented in this research showed to be adequate to quantify the propagating and allylic free radicals separately in samples of dimethacrylate resin-based dental materials, opening new possibilities to probe the radical's kinetics. With this methodology, we found that that the allylic radical's half-life time is approximately twice than that for the propagating radical, independently the initiation mode and material's composition. In addition, the findings suggest that their relative reactivity is constant as well. These results give new insights into the understanding of the polymerization process of resin-based dental materials and highlight the relevance of using ESR spectroscopy.

References

1. Sideridou ID, Achilias DS (2005) Elution study of unreacted Bis-GMA, TEGDMA, UDMA, and Bis-EMA from light-cured dental resins and resin composites using HPLC. J Biomed Mater Res Part B Appl Biomater 74:617–626. https://doi.org/10.1002/jbm.b.30252
2. Leprince JG, Palin WM, Hadis MA et al (2013) Progress in dimethacrylate-based dental composite technology and curing efficiency. Dent Mater 29:139–156. https://doi.org/10.1016/j.dental.2012.11.005
3. Ferracane JL (2011) Resin composite—state of the art. Dent Mater 27:29–38. https://doi.org/10.1016/j.dental.2010.10.020
4. Sideridou I, Tserki V, Papanastasiou G (2002) Effect of chemical structure on degree of conversion in light-cured dimethacrylate-based dental resins. Biomaterials 23:1819–1829. https://doi.org/10.1016/s0142-9612(01)00308-8
5. Salomão FM, Vicentin BLS, Contreras EFR et al (2015) The influence of a translucent fiberglass post on the polymerization of dual cure resin cement analyzed by electron paramagnetic resonance. Mater Res 18:1023–1028. https://doi.org/10.1590/1516-1439.022115
6. Jakubiak J, Allonas X, Fouassier JP et al (2003) Camphorquinone-amines photoinitating systems for the initiation of free radical polymerization. Polymer (Guildf) 44:5219–5226. https://doi.org/10.1016/s0032-3861(03)00568-8
7. Ikemura K, Endo T (2010) A review of the development of radical photopolymerization initiators used for designing light-curing dental adhesives and resin composites. Dent Mater J 29:481–501. https://doi.org/10.4012/dmj.2009-137
8. Nie J, Andrzejewska E, Rabek JF et al (1999) Effect of peroxides and hydroperoxides on the camphorquinone-initiated photopolymerization. Macromol Chem Phys 200:1692–1701. https://doi.org/10.1002/(sici)1521-3935(19990701)200:7%3c1692:aid-macp1692%3e3.0.co;2-r
9. Teshima W, Nomura Y, Tanaka N et al (2003) ESR study of camphorquinone/amine photoinitiator systems using blue light-emitting diodes. Biomaterials 24:2097–2103. https://doi.org/10.1016/s0142-9612(02)00636-1
10. Kwon TY, Bagheri R, Kim YK et al (2012) Cure mechanisms in materials for use in esthetic dentistry. J Investig Clin Dent 3:3–16. https://doi.org/10.1111/j.2041-1626.2012.00114.x
11. Truffier-Boutry D, Gallez XA, Demoustier-Champagne S et al (2003) Identification of free radicals trapped in solid methacrylated resins. J Polym Sci Part A Polym Chem 41:1691–1699. https://doi.org/10.1002/pola.10692
12. Vicentin BLS, Salomão FM, Hoeppner MG, Di Mauro E (2016) Influence of geometrical configuration of a translucent fiberglass post on the polymerization of a dual cure resin cement analyzed by EPR spectroscopy. Appl Magn Reson 47:211–222. https://doi.org/10.1007/s00723-015-0740-x
13. Anseth KS, Anderson KJ, Bowman CN (1996) Radical concentrations, environments, and reactivities during crosslinking polymerizations. Macromol Chem Phys 197:833–848. https://doi.org/10.1002/macp.1996.021970306

14. Da Fontes AS, Vicentin BLS, Valezi DF et al (2014) A multifrequency (X-, Q-, and W-band) EPR and DFT study of a photopolymerizable dental resin. Appl Magn Reson 45:681–692. https://doi.org/10.1007/s00723-014-0546-2

15. Vicentin BLS, Netto AM, Blümich B, Di Mauro E (2016) Identification of free radicals generated by different curing modes in a dental resin cement. Appl Magn Reson 47:1003–1014. https://doi.org/10.1007/s00723-016-0803-7

16. Leprince JG, Lamblin G, Devaux J et al (2010) Irradiation modes' impact on radical entrapment in photoactive resins. J Dent Res 89:1494–1498. https://doi.org/10.1177/0022034510384624

17. Bunce NJ (1987) Introduction to the interpretation of electron spin resonance spectra of organic radicals. J Chem Educ 64:907. https://doi.org/10.1021/ed064p907

18. Gerson F, Huber W (2003) Electron spin resonance spectroscopy of organic radicals, 1o edn. WILEY-VCH Verlag GmbH & Co., KGaA, Weinheim

19. Ottaviani MF, Fiorini A, Mason PN, Corvaja C (1992) Electron spin resonance studies of dental composites: effects of irradiation time, decay over time, pulverization, and temperature variations. Dent Mater 8:118–124. https://doi.org/10.1016/0109-5641(92)90066-l

20. Fontes ADS, Di Mauro E, Sano W et al (2009) Avaliação do comportamento de radicais livres e desempenho mecânico de compósitos restauradores dentais comerciais por Ressonância Paramagnética Eletrônica (RPE) combinada às análises convencionais. Polímeros 19:285–291. https://doi.org/10.1590/s0104-14282009000400007

21. Da Fontes AS, Sano W, Antonia LHD, Di Mauro E (2010) EPR in the characterization of the shade effect on translucence, remaining free radicals, and polymerization depth of commercially available resin composites. Appl Magn Reson 39:381–390. https://doi.org/10.1007/s00723-010-0172-6

22. Vicentin BLS, Netto AM, Dall'Antonia LH et al (2017) Real-time polymerization monitoring in a dual-cured resin cement by magnetic resonance. Polym Bull 74:5163–5179. https://doi.org/10.1007/s00289-017-2007-1

23. Lamblin G, Devaux J, Biebuyck J (2007) Electron spin resonance, a useful analytical technique for studying the kinetic decay of free radicals trapped in dental resin. Eur Cells Mater 13:2262

24. Leprince J, Lamblin G, Truffier-Boutry D et al (2009) Kinetic study of free radicals trapped in dental resins stored in different environments. Acta Biomater 5:2518–2524. https://doi.org/10.1016/j.actbio.2009.04.034

25. Truffier-Boutry D, Demoustier-Champagne S, Devaux J et al (2006) A physico-chemical explanation of the post-polymerization shrinkage in dental resins. Dent Mater 22:405–412. https://doi.org/10.1016/j.dental.2005.04.030

26. Fonseca R, Santos C, Adabo L (2004) The influence of chemical activation on hardness of dual-curing resin cements a influência da ativação química na dureza de cimentos resinosos duais. Braz Oral Res 18:228–232. https://doi.org/10.1590/S1806-83242004000300009

27. Arrais CAG, Kasaz ADC, Albino LGB et al (2010) Effect of curing mode on the hardness of dual-cured composite resin core build-up materials. Braz Oral Res 24:245–249. https://doi.org/10.1590/s1806-83242010000200019

28. Burey A, dos Reis PJ, Santana Vicentin BL et al (2018) Polymerization shrinkage and porosity profile of dual cure dental resin cements with different adhesion to dentin mechanisms. Microsc Res Tech 81:88–96. https://doi.org/10.1002/jemt.22960